Inherently Robust Micromachined Gyroscopes With 2-DOF Sense-Mode Oscillator

Cenk Acar, *Member, IEEE, Member, ASME,* and Andrei M. Shkel, *Associate Member, IEEE, Associate Member, ASME*

***Abstract*—Commercialization of reliable vibratory micromachined gyroscopes for high-volume applications has proven to be extremely challenging, primarily due to the high sensitivity of the dynamical system response to fabrication and environmental variations. This paper reports a novel micromachined gyroscope with two degrees-of-freedom (DOF) sense-mode oscillator that provides inherent robustness against structural parameter variations. The 2-DOF sense-mode oscillator provides a frequency response with two resonant peaks and a flat region between the peaks, instead of a single resonance peak as in conventional gyroscopes. The device is nominally operated in the flat region of the sense-mode response curve, where the amplitude and phase of the response are insensitive to parameter fluctuations. Furthermore, the sensitivity is improved by utilizing dynamical amplification of oscillations in the 2-DOF sense-mode oscillator. Thus, improved robustness to variations in temperature, damping, and structural parameters is achieved, solely by the mechanical system design. Prototype gyroscopes were fabricated using a bulk-micromachining process, and the performance and robustness of the devices have been experimentally evaluated. With a 25 V dc bias and 3 V ac drive signal resulting in 5.8 μm drive-mode amplitude, the gyroscope exhibited a measured noise-floor of $0.64^\circ/s/\sqrt{Hz}$ over 50 Hz bandwidth in atmospheric pressure. The sense-mode response in the flat operating region was also experimentally demonstrated to be inherently insensitive to pressure, temperature, and dc bias variations. [1501]**

***Index Terms*—Inertial sensor, MEMS gyroscope, micromachined gyroscope, rate sensor.**

I. Introduction

SINCE the first demonstration of a micromachined gyroscope by the Draper Laboratory in 1991 [1], various micromachined gyroscope designs fabricated in surface micromachining, bulk micromachining, hybrid surface-bulk micromachining technologies, or alternative fabrication techniques have been reported [2]–[4]. Inspired by the promising success of micromachined accelerometers in the same era, extensive research efforts toward commercial micromachined gyroscopes led to several innovative gyroscope topologies, fabrication and integration approaches, and detection techniques. Consequently, vibratory micromachined gyroscopes that utilize vibrating elements to induce and detect Coriolis force have been proven to be effectively implemented and batch fabricated in different micromachining processes. However, achieving robustness against fabrication variations and temperature fluctuations remains one of the greatest challenges in commercialization and high-volume production of micromachined vibratory rate gyroscopes.

In most of the reported microelectromechanical systems (MEMS) gyroscopes, a two degrees-of-freedom (2-DOF) mass-spring-damper system is formed, and the proof mass is driven into resonance in the drive direction. Typically, the sense mode is designed to be slightly shifted from the drive mode in order to improve bandwidth, robustness, and thermal stability, while intentionally sacrificing gain and sensitivity. Yet, the response amplitude and phase of the resulting mechanical system remains extremely sensitive to the relative location of the drive and sense resonant frequencies. The inadequate tolerancing and critical dimension control capabilities of the current photolithography processes and microfabrication techniques lead to drastic variations in oscillatory system parameters. Thus, the resulting fabrication variations and imperfections that shift the natural frequencies impose strict requirements for the active feedback control system and the detection electronics [5]–[7].

This paper presents a novel structural design concept for micromachined gyroscopes that provide inherent robustness against structural and environmental parameter variations. The emphasis is on investigating the paradigm of shifting the complexity from the control electronics to the structural design of gyroscope dynamical system. The design approach explores the possibility of achieving a wide-bandwidth frequency response in the sense mode of the vibratory gyroscopes. Thus, the disturbance-rejection capability is achieved by the mechanical system instead of active control and compensation strategies [8], [9]. The micromachined gyroscopes of this class could potentially yield reliable, robust, and high-performance angular-rate measurements leading to a wide range of high-volume applications including dynamic vehicle control, automotive safety systems, navigation/guidance systems, and interactive consumer electronics.

II. The 3-DOF Micromachined Gyroscope Structure

The presented design concept addresses the following major MEMS gyroscope design challenges:

1) the requirement of precisely controlling the relative location of the drive and sense resonance modes from die to die, from wafer to wafer, and within the required temperature range;
2) variation in the Coriolis signal phase due to the shift in natural frequencies;

Manuscript received January 10, 2005; revised June 23, 2005. Subject Editor G. B. Hocker.

C. Acar was with the Mechanical and Aerospace Engineering Department, MicroSystems Laboratory, University of California, Irvine, Irvine, CA 92697 USA. He is now with BEI Technologies, Systron Donner Automotive Division, Concord, CA 94518 USA (e-mail: cacar@systron.com).

A. M. Shkel is with the Mechanical and Aerospace Engineering Department, MicroSystems Laboratory, University of California, Irvine, Irvine, CA 92697 USA (e-mail: ashkel@uci.edu).

Digital Object Identifier 10.1109/JMEMS.2006.872224

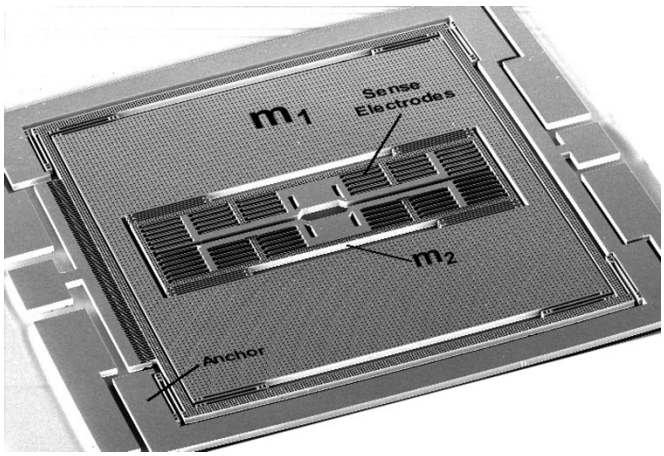

Fig. 1. Scanning electron micrograph of the prototype bulk-micromachined 3-DOF gyroscope with 2-DOF sense mode.

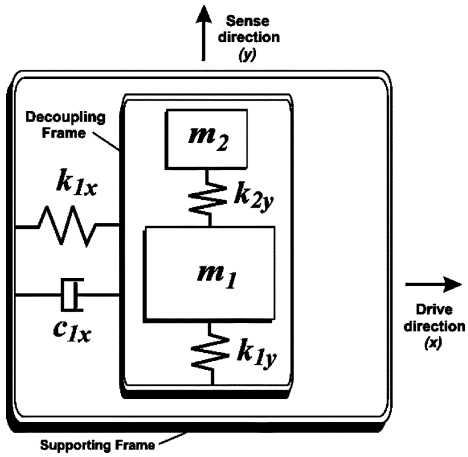

Fig. 2. Lumped mass-spring-damper model of the overall 3-DOF gyroscope with 2-DOF sense mode.

3) long-term variation in sensitivity due to packaging pressure degradation over time;
4) minimizing the quadrature error and bias due to mechanical coupling between the drive and sense modes.

The proposed gyroscope dynamical system consists of a 2-DOF sense-mode oscillator and a 1-DOF drive-mode oscillator, formed by two interconnected proof masses (see Fig. 1). The first mass m_1 is free to oscillate both in the drive and the sense directions and is excited in the drive direction. The second mass m_2 is constrained in the drive direction with respect to the first mass. In the drive direction, m_1 and m_2 oscillate together and form a resonant 1-DOF oscillator. The smaller proof mass m_2 forms the passive mass of the 2-DOF sense-mode oscillator (see Fig. 2) and acts as the vibration absorber to dynamically amplify the sense mode oscillations of m_1.

The 2-DOF sense-mode oscillator provides a frequency response with two resonant peaks and a flat region between the peaks, instead of a single resonance peak as in conventional gyroscopes (see Fig. 3). The device is nominally operated in the flat region of the sense-mode response curve, where the gain is less sensitive to variations in the natural frequencies and damping. Thus, reduced sensitivity to structural and thermal parameter fluctuations and damping changes is achieved, leading to improved long-term stability and robustness against temperature variations and fabrication variations from device to device.

Furthermore, the sensitivity is improved by utilizing dynamical amplification of oscillations in the 2-DOF sense-mode oscillator [14]. The smaller mass m_2 is employed as the sensing mass, and the larger mass m_1 generates the Coriolis force that excites the 2-DOF sense-mode oscillator. For a given Coriolis force, the amplitude of the sensing mass m_2 increases with decreasing ratio of the proof masses m_2/m_1, which dictates minimizing the mass of m_2 and maximizing the mass of m_1. Also, it is desired that a large Coriolis force is induced on m_1, which also dictates maximizing the mass of m_1. With these two aligning major design constraints, the concept could potentially yield better sensitivity than a conventional gyroscope with mismatched modes while providing enhanced robustness.

Since the gyroscope structure oscillates as a 1-DOF resonator in the drive direction, the frequency response of the device has a single resonance peak in the drive mode. The device is operated at resonance in the drive mode, while the wide-bandwidth frequency region is obtained in the sense-mode frequency response. Thus, the flat region of the sense-mode oscillator is designed to coincide with the drive-mode resonant frequency. This allows utilization of well-proven drive-mode control techniques, while providing robust gain and phase in the sense mode.

A. Mode Decoupling

Fabrication imperfections and residual stresses in MEMS gyroscopes generally introduce small imbalances and asymmetries in the gyroscope suspension structure. Due to lack of perfect alignment of the intended and the actual principle axes of oscillation, anisoelasticity in the gyroscope structure occurs, causing dynamic cross-coupling between the drive and sense directions [11]–[13]. This results in mechanical interference between the modes, often much larger than the Coriolis motion. This undesired coupling, called quadrature error, is in phase with the proof-mass displacement, and 90° phase shifted from the Coriolis force proportional to the proof-mass velocity. Even though phase-sensitive detection techniques can partially discriminate the quadrature error, the device performance degrades.

In the 3-DOF gyroscope structure, the drive and sense direction oscillations of m_1 can be mechanically decoupled to a great extent by using a unidirectional frame structure, in order to minimize quadrature error and undesired electrostatic forces in the sense mode due to drive-mode actuator imperfections. When m_1 is nested inside a drive-mode frame (see Fig. 4), the sense-direction oscillations of the frame are constrained and the drive-direction oscillations are automatically forced to be in the designed drive direction.

Thus, possible anisoelasticities due to fabrication imperfections are suppressed. Since m_1 is free to oscillate only in the sense direction with respect to the frame, the sense-mode response of m_1 is assured to be perfectly orthogonal to the drive direction.

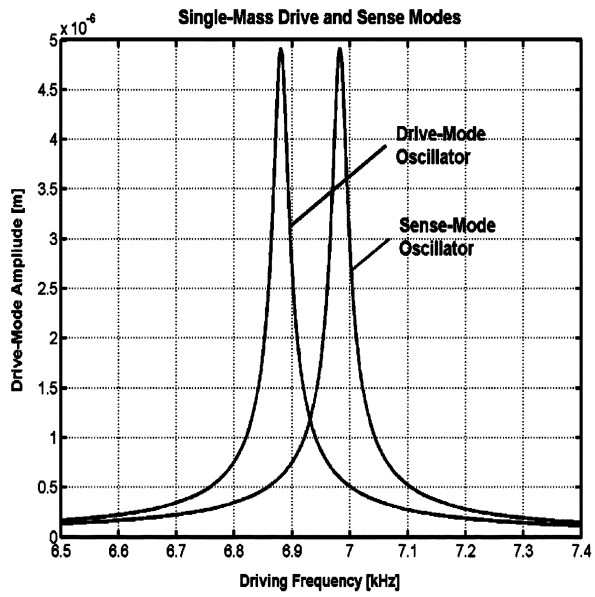

Conventional Gyroscopes

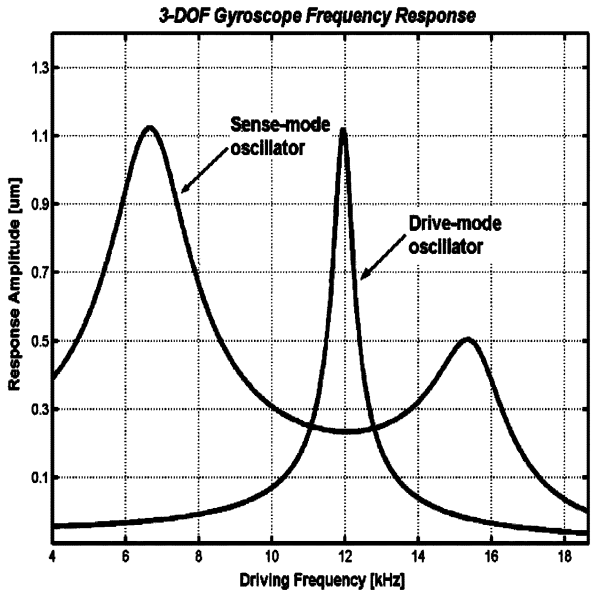

3-DOF Design Concept

Fig. 3. Frequency response comparison of the single-mass conventional gyroscopes and the disclosed robust micromachined gyroscope with 2-DOF sense-mode oscillator.

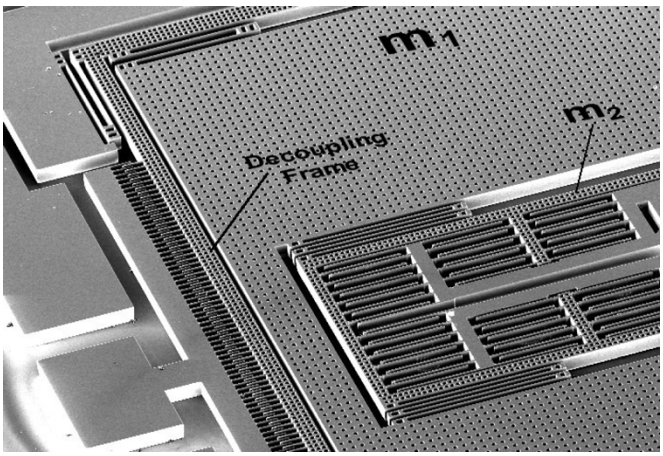

Fig. 4. The frame implementation for decoupling the drive and sense-mode oscillations of m_1.

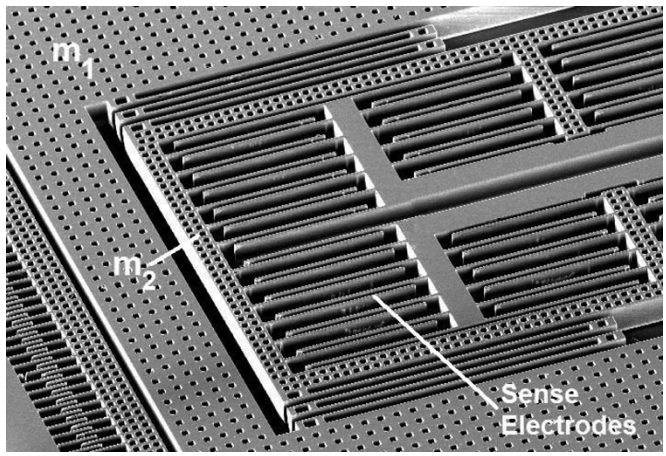

Fig. 5. Scanning electron micrograph of the sense-mode passive mass m_2 and the differential sensing electrodes.

III. Gyroscope Dynamics

The 3-DOF gyroscope dynamical system is analyzed in the noninertial coordinate frame associated with the gyroscope. Each of the interconnected proof masses is assumed to be a rigid body with a position vector $\vec{r}$ attached to a rotating gyroscope reference frame B with an angular velocity of $\vec{\Omega}$, resulting in an absolute acceleration in the inertial frame A

$$\vec{a_A} = \vec{a_B} + \dot{\vec{\Omega}} \times \vec{r_B} + \vec{\Omega} \times (\vec{\Omega} \times \vec{r_B}) + 2\vec{\Omega} \times \vec{v_B} \quad (1)$$

where $\vec{v_B}$ and $\vec{a_B}$ are the velocity and acceleration vectors with respect to the reference frame B, respectively. Thus, the equations of motion of m_1 and m_2 can be expressed in the inertial frame as

$$m_1\vec{a_1} = \vec{F_1} + \vec{F_d} + \vec{F_r} - 2m_1\vec{\Omega} \times \vec{v_1} - m_1\vec{\Omega} \times (\vec{\Omega} \times \vec{r_1}) - m_1\dot{\vec{\Omega}} \times \vec{r_1} \quad (2)$$

$$m_2\vec{a_2} = \vec{F_2} - \vec{F_r} - 2m_2\vec{\Omega} \times \vec{v_2} - m_2\vec{\Omega} \times (\vec{\Omega}\vec{r_2}) - m_2\dot{\vec{\Omega}} \times \vec{r_2} \quad (3)$$

where $\vec{F_d}$ is the driving force applied on m_1, $\vec{F_1}$ is the net external force applied to m_1 including elastic and damping forces from the substrate, $\vec{F_2}$ is the net external force applied to m_2 including the damping force from the substrate, and $\vec{F_r}$ is the elastic reaction force between m_1 and m_2. In the gyroscope frame, $\vec{r_1}$ and $\vec{r_2}$ are the position vectors and $\vec{v_1}$ and $\vec{v_2}$ are the velocity vectors of m_1 and m_2, respectively.

The following constraints and assumptions further simplify the dynamics of the 3-DOF system. The structure is stiff in the out-of-plane direction; the position vector of the decoupling frame is forced to lie along the drive direction; m_1 oscillates purely in the sense direction relative to the decoupling frame; m_1 and m_2 move together in the drive direction ($x_1 = x_2$); and m_2 oscillates purely in the sense direction relative to m_1. Thus,

the equations of motion of m_1 and m_2 are decomposed into the drive and sense directions to yield

$$(m_1+m_2+m_f)\ddot{x_1}+c_{1x}\dot{x_1}+k_{1x}x_1 = (m_1+m_2+m_f)\Omega_z^2 x_1+F_d(t) \quad (4)$$

$$m_1\ddot{y_1}+c_{1y}\dot{y_1}+k_{1y}y_1 = k_{2y}(y_2-y_1)+m_1\Omega_z^2 y_1 - 2m_1\Omega_z\dot{x_1}-m_1\dot{\Omega}_z x_1 \quad (5)$$

$$m_2\ddot{y_2}+c_{2y}\dot{y_2}+k_{2y}y_2 = k_{2y}y_1+m_2\Omega_z^2 y_2-2m_2\Omega_z\dot{x_2}-m_2\dot{\Omega}_z x_2 \quad (6)$$

where Ω_z is the z-axis angular rate, m_f is the mass of the decoupling frame, and $F_d(t)$ is the driving electrostatic force applied to the active mass at the driving frequency ω_d. The Coriolis force that excites m_1 and m_2 in the sense direction is $2m_1\Omega_z\dot{x_2}$, and the Coriolis response of m_2 in the sense direction (y_2) is detected for angular rate measurement.

IV. Experimental Evaluation

A. Bulk-Micromachined Prototype Design

Prototype 3-DOF gyroscope structures were fabricated in the UCI Integrated Nano-Systems Research Facility using a one-mask bulk-micromachining process, based on deep-reactive ion etching (DRIE) through the 100 μm device layer of silicon-on-insulator wafers. The DRIE process was performed in an STS inductively coupled plasma (ICP), using an 8 s etch step cycle with 130 sccm SF_6 and 13 sccm O_2, 600 W coil power and 15 W platen power; and 5 sec passivation step cycle time with 85 sccm C_4F_6, 600 W coil power, and 0 W platen power. In the device, 15 $\times$15 μm^2 holes were used to perforate the suspended structures, in order to allow front-side release of the structures by etching the oxide layer in HF solution. The anchors were designed as unperforated areas larger than 40 $\times$40 μm^2 for 25 min release in 49% HF solution, defining the structural layer and the anchor layer using one mask.

The dynamical system parameters of the prototype 3-DOF gyroscope with 2-DOF sense mode are as follows. The proof mass values are $m_1 = 2.46\times10^{-6}$ kg, $m_2 = 1.54\times10^{-7}$ kg, and the decoupling frame mass $m_f = 1.19\times10^{-7}$ kg. The spring constants are $k_{1x} = 61.2$ N/m, $k_{1y} = 78.4$ N/m, and $k_{2y} = 3.36$ N/m. The overall device size is approximately 4×4 mm^2.

For the 1-DOF drive-mode oscillator, the effective proof-mass value becomes $m_{1x} = (m_1+m_2+m_f) = 2.74\times10^{-6}$ kg. This yields a drive-mode resonant frequency of 752 Hz.

In the sense mode, the resonant frequencies of the isolated active and passive mass-spring systems are $\omega_{1y}=\sqrt{k_{1y}/m_1}=897.7$ Hz and $\omega_{2y}=\sqrt{k_{2y}/m_2}=732.2$ Hz, respectively; yielding a frequency ratio of $\gamma_y=\omega_{2y}/\omega_{1y}=0.897$, and a mass ratio of $\mu_y=m_2/m_1=0.0624$. With these parameters, the location of the two expected resonance peaks in the sense-mode frequency response was calculated as $f_{y-n1}=696.7$ Hz and $f_{y-n2}=943.3$ Hz, based on the relation

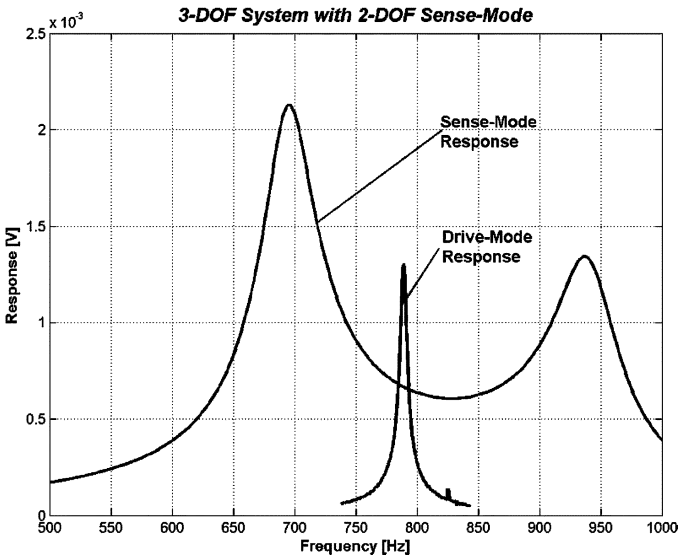

Fig. 6. Experimental measurements of the drive- and sense-mode frequency responses, demonstrating that the drive-mode resonant frequency is located inside the sense-mode flat region.

$$\omega_{y-n1} = \sqrt{\frac{1}{2}\left(1+\mu_y+\frac{1}{\gamma_y^2}-\sqrt{\left(1+\mu_y+\frac{1}{\gamma_y^2}\right)^2-\frac{4}{\gamma_y^2}}\right)}\times\omega_{2y} \quad (7)$$

$$\omega_{y-n2} = \sqrt{\frac{1}{2}\left(1+\mu_y+\frac{1}{\gamma_y^2}+\sqrt{\left(1+\mu_y+\frac{1}{\gamma_y^2}\right)^2-\frac{4}{\gamma_y^2}}\right)}\times\omega_{2y}. \quad (8)$$

B. Experimental Results

The frequency responses of the 2-DOF sense-mode oscillator and the 1-DOF drive-mode oscillator of the prototype 3-DOF gyroscope were characterized under atmospheric pressure in an MMR probe station. For the sense-mode characterization, one-port actuation and detection was utilized, where one probe was used to impose the driving ac signal plus the dc bias voltage on the gyroscope structure and one probe was contacted with the sensing electrode of the sense-mode passive mass m_2. Thus, the extracted sense-mode frequency response reflects the case where the excitation force is applied on the passive mass instead of the active mass. The acquired sense-mode frequency response was then numerically postprocessed [8] in order to obtain the actual response of the passive mass when the active mass is excited by the Coriolis force.

In the resulting sense-mode frequency response, a flat region of over 200 Hz was experimentally demonstrated (see Fig. 6).

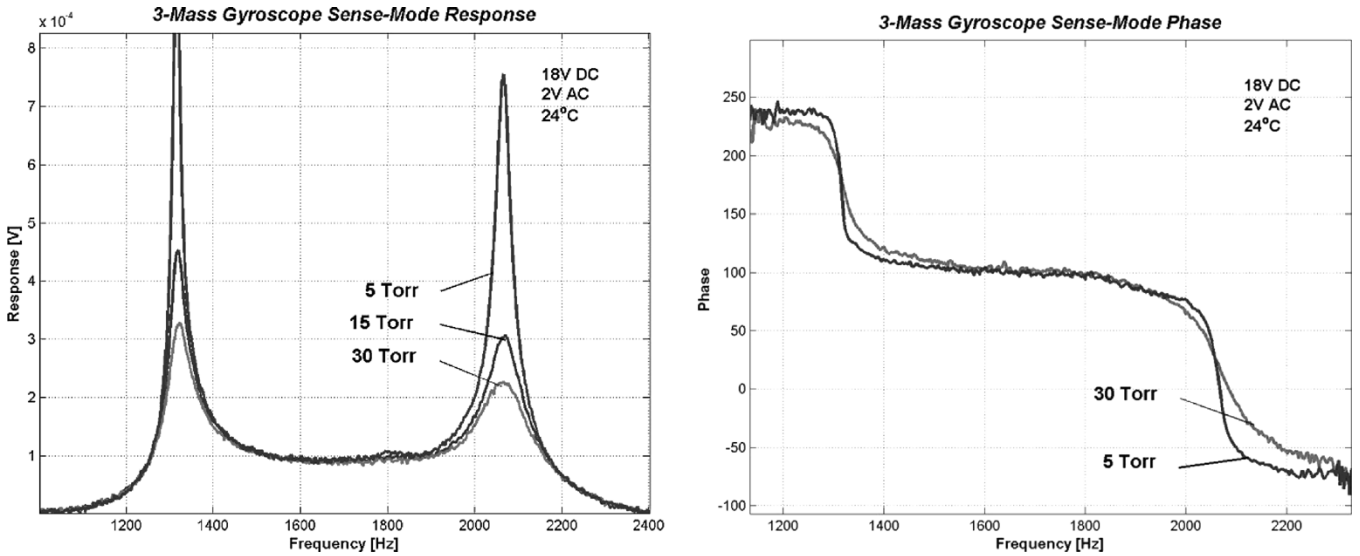

Fig. 7. Electrostatically acquired amplitude and phase response, with changing pressure values. The amplitude and phase of the response remains constant within the flat region.

The two resonance peaks in the drive-mode frequency response were observed as $f_{y-n1} = 693$ Hz and $f_{y-n2} = 940$ Hz, in very good agreement with the theoretically estimated values of $f_{y-n1} = 696.7$ Hz and $f_{y-n2} = 943.3$ Hz. When the drive- and sense-mode frequency responses of the prototype 3-DOF gyroscope were investigated together, the drive-mode resonant frequency was observed to be located inside the sense-mode flat region as desired (see Fig. 6), allowing the gyroscope to be operated at resonance in the drive mode and within the flat region in the sense mode.

V. Experimental Analysis of Parametric Sensitivity

In order to characterize the frequency response of the 2-DOF sense-mode oscillator under different pressure and temperature conditions, electrostatic actuation and capacitive detection were utilized in an MMR vacuum probe station. A test gyroscope structure similar to the 2-DOF sense-mode oscillator of the gyroscope, but with actuation electrodes attached to the sense-mode active mass m_1, was designed and characterized. The frequency response was acquired using off-chip transimpedance amplifiers with a feedback resistor of $R_A = 1\ \mathrm{M}\Omega$ connected to an HP signal analyzer in sine-sweep mode. Two-port actuation and detection was utilized, where one probe was used to impose the dc bias voltage on the gyroscope structure through the anchor, one probe was used to apply the ac drive voltage on the actuation port attached to the active mass m_1, and the detection port on the passive mass m_2 was directly connected to the transimpedance amplifier.

A. Pressure Variations

Fig. 7 presents the experimentally measured amplitude and phase responses of the sense-mode passive mass at 5, 15, and 30 Torr acquired in an MMR vacuum probe station. The oscillation amplitude in the two resonance peaks were observed to increase with decreasing pressures. However, the change in the response amplitude in the flat operating region is insignificant, as anticipated by the theoretical analysis. This experimentally demonstrates the damping insensitivity of the sense-mode response in the flat operating region, as desired.

Furthermore, the phase of the sense-mode passive mass was observed to stay constant in the operating frequency band, while the phase changes were observed at the two resonance peaks as expected (see Fig. 7). Thus, it is experimentally verified that a constant-phase response is achieved in the operating region, in contrast to the abrupt phase changes around the resonance peaks as in the conventional gyroscopes.

B. Temperature Variations

The sensitivity of the prototype gyroscopes to temperature variations was characterized by heating the vacuum chamber of the MMR probe station and continuously monitoring the temperature of the sample using a solid-state temperature sensor attached to the handle wafer.

Fig. 8 presents the capacitively acquired frequency response of the sensing element at the temperatures 25 °C and 75 °C. The maximum amplitude variation in the flat operating region was observed to be less than 2% for the 50 °C variation in temperature, experimentally verifying the improved robustness against temperature variations.

When the change in the response gain at the resonance peaks is considered (see Fig. 9), it is observed that the frequency shift due to the temperature change results in a maximum of over 40% drop in the gain. The response amplitude in the flat operating region is observed to remain unchanged also in Fig. 9.

C. Electrostatic Tuning

In order to observe the effects of larger stiffness variations on the system response, the frequency response of the sense-

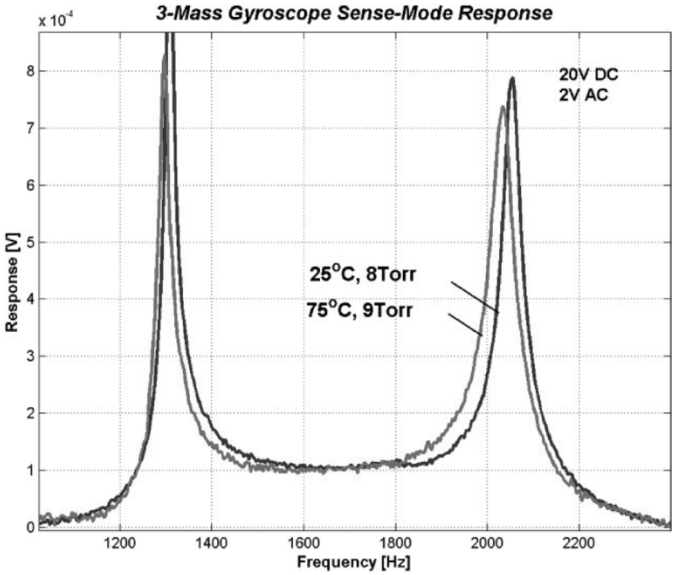

Fig. 8. The frequency response of the sense-mode passive mass at 25 and 75 °C. The response gain within the flat operating region is observed to stay constant.

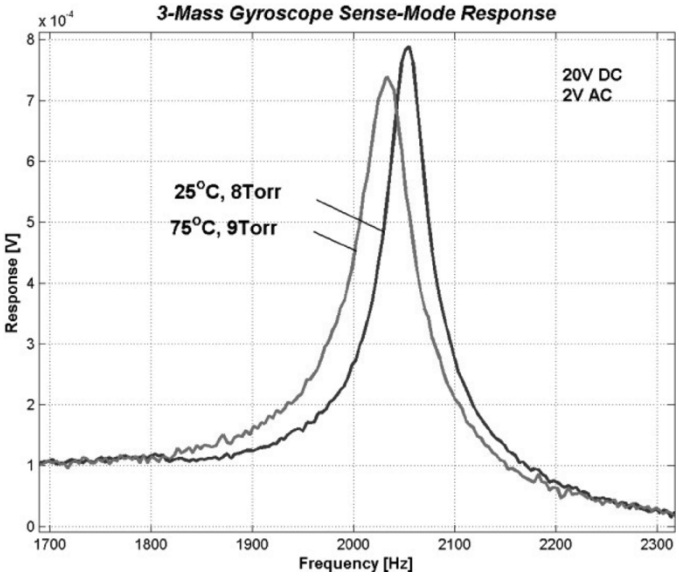

Fig. 9. Closeup of the frequency response of the sense-mode passive mass at 25 and 75 °C, showing the frequency shift at the second resonance peak and the constant response at the flat operating region.

mode passive mass was acquired with different dc bias voltages. Fig. 10 presents the experimental frequency response measurements for 18–21 V dc bias at 4 torr pressure. The electrostatic negative spring effect was observed to result in 30 Hz shift in the first resonance peak and 45 Hz shift in the second resonance peak; however, the response amplitude in the flat operating region was observed to change insignificantly.

VI. Rate-Table Characterization

The 3-DOF gyroscope sample was diced and packaged in a ceramic dual in-line package (DIP) package by direct wire-bonding to the proof-mass anchor, center sense electrode, and drive electrode bonding pads. Synchronous demodulation technique was used to extract the angular rate response of the 3-DOF system with 2-DOF sense mode. The drive signal applied on the comb-drive actuators was 25 V dc bias and 3 V ac. The device was operated at resonance in the drive mode, at 752 Hz, without utilizing active drive-mode control. The drive-mode amplitude was measured optically during the operation of the device as 5.8 μm, using a microscope attached to the rate-table platform.

A 20-kHz carrier signal was imposed on the gyroscope structure, and the output from the differential sense capacitors was amplified outside the package and synchronously amplitude demodulated at the carrier signal frequency using a lock-in amplifier. The Coriolis signal was finally demodulated at the driving frequency.

With this technique, a sensitivity of 0.0308 $\mathrm{mV}/(^0/\mathrm{s})$ was experimentally demonstrated while the device was operated in the flat region of the sense-mode frequency response (see Fig. 11). The measured noise floor was 19.7 $\mu\mathrm{V}/\sqrt{\mathrm{Hz}}$ at 50 Hz bandwidth, yielding a measured resolution of $0.64^0/\mathrm{s}/\sqrt{\mathrm{Hz}}$ at 50 Hz bandwidth in atmospheric pressure. The majority of the noise originates from the use of external electronics. Future implementations could drastically improve the resolution by utilizing direct connections to preamplifiers or complete detection electronics inside the device package.

A. Experimental Verification of Improved Robustness

In order to verify that robustness to parameter variations is achieved in the overall Coriolis response of a wide-bandwidth gyroscope, the 3-DOF gyroscope structure with 2-DOF sense mode was characterized on the rate table in a thermally controlled chamber.

When the temperature of the gyroscope was increased from 25 to 75 °C while keeping the excitation frequency constant at 752 Hz, the sensitivity of the gyroscope was observed to drop from 0.0308 to 0.0234 $\mathrm{mV}/(^0/\mathrm{s})$. This translates into a 24.1% drop in the response gain. When the change in the drive-mode amplitude from 25 to 75 °C was investigated, it was seen that it changed from 5.8 to 4.3 μm, yielding a 25.9% decrease. Thus, it was concluded that the change in the gyroscope sensitivity was almost purely due to the drive-mode amplitude change (with 1.8% discrepancy); verifying the insensitivity of the sense-mode response to temperature variations.

In order to confirm this result, the rate table characterization at 75 °C was repeated, this time changing the drive frequency to 750 Hz. At this frequency, the drive-mode amplitude was restored to 5.8 μm, and a sensitivity of 0.0303 $\mathrm{mV}/(^0/\mathrm{s})$ was measured using the least squares fit line (see Fig. 12). Consequently, it was experimentally demonstrated that a temperature variation from 25 to 75 °C results in only 1.62% change in the output of the wide-bandwidth gyroscope approach, verifying the improved robustness. At elevated temperatures, the linearity of the response was also observed to be preserved.

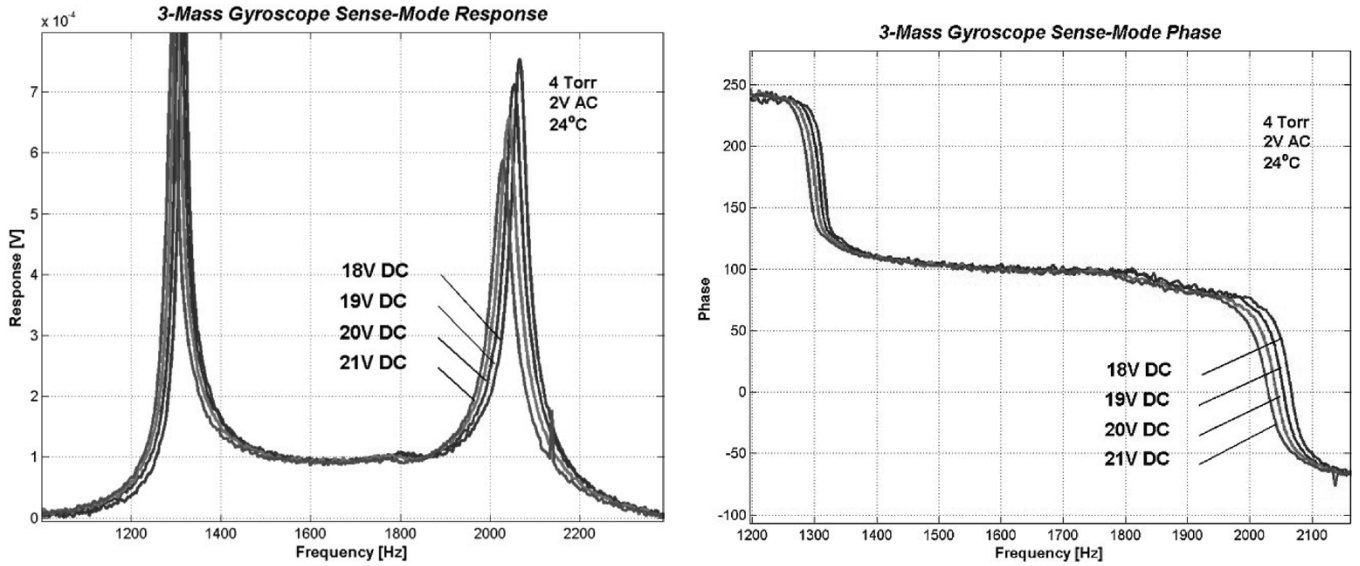

Fig. 10. Electrostatically detected amplitude and phase response of the sense-mode passive mass with changing dc bias.

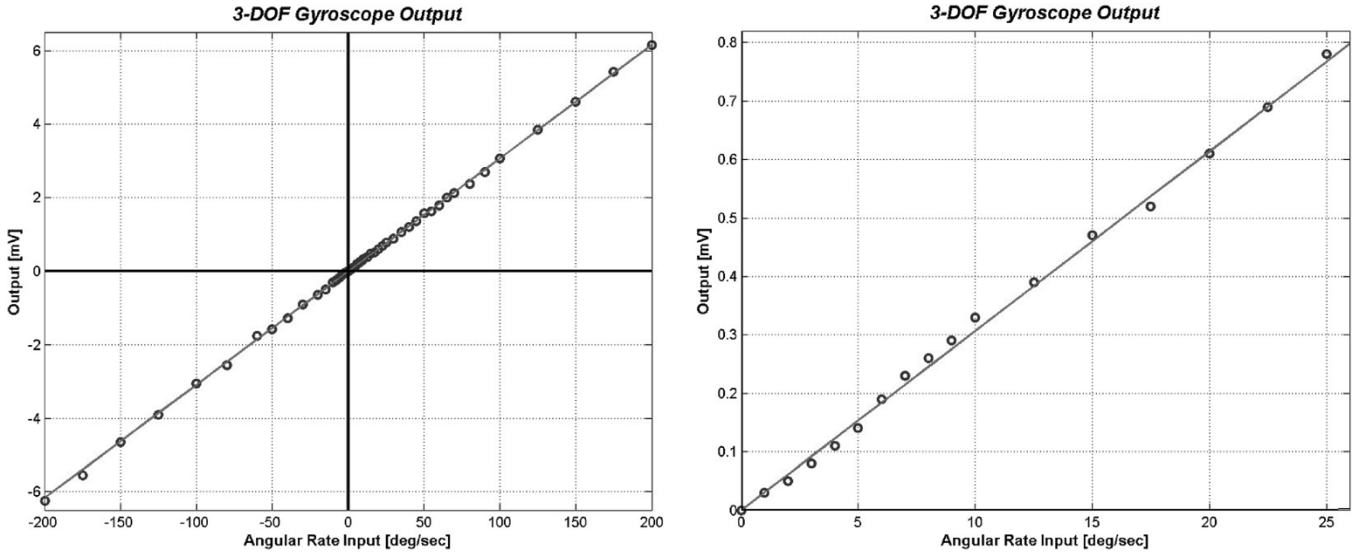

Fig. 11. The angular-rate input versus voltage output plot obtained from the 3-DOF gyroscope with 2-DOF sense mode in the -200 to $200^\circ/\mathrm{s}$ and 0 to $+25^\circ/\mathrm{s}$ input ranges. The scale factor is obtained as $0.0308\ \mathrm{mV}/(^0/\mathrm{s})$ from the least squares fit line.

B. Comparison of Response With a Conventional Gyroscope

In order to compare the improved robustness of the proposed wide-bandwidth approach, a micromachined gyroscope with a conventional 1-DOF sense mode was fabricated on the same wafer, and characterized under the same temperature variations and using the same signal conditioning electronics.

When the temperature of the tested conventional gyroscope was increased from 25 to 75 °C while restoring the drive-mode amplitude to 12 μm, the sensitivity was observed to drop from 0.91 to $0.73\ \mathrm{mV}/(^0/\mathrm{s})$. Thus, a 50 °C temperature increase was observed to result in 19.8% sensitivity change in the conventional gyroscope, which is over 12.2 times larger than the 3-DOF gyroscope approach.

VII. Conclusion

This paper presented a 3-DOF gyroscope system with 2-DOF sense-mode oscillator, which significantly suppresses the effect of parameter variations on the gain and phase of the sense-mode response, while compatible with well-proven drive-mode control techniques. The in-house fabricated bulk-micromachined prototypes were successfully operated as a gyroscope in the flat region of the sense-mode response. The prototype gyroscope exhibited a measured noise floor of $0.64^\circ/\mathrm{s}/\sqrt{\mathrm{Hz}}$ over 50 Hz bandwidth in atmospheric pressure. The sense-mode response in the flat operating region was also experimentally demonstrated to be inherently insensitive to pressure, temperature, and dc bias variations. The results of this work introduce and demonstrate a new paradigm in MEMS gyroscope design,

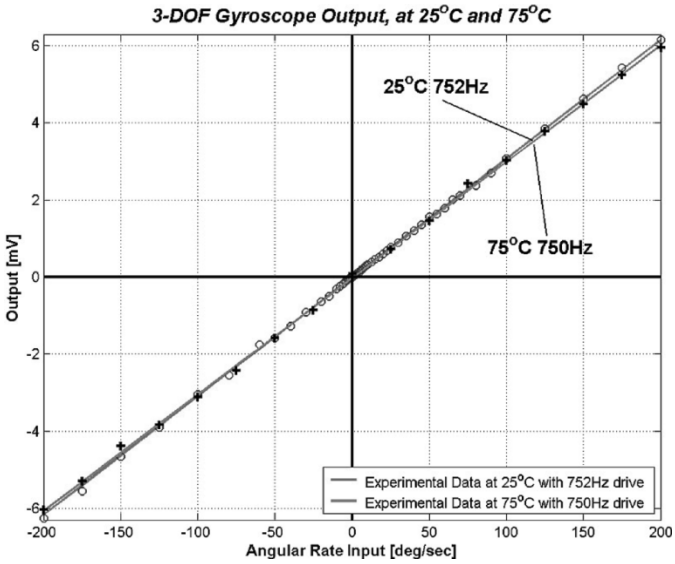

Fig. 12. The measured angular-rate response of the 3-DOF gyroscope at 25 and 75 °C when the drive frequency is changed from 752 to 750 Hz.

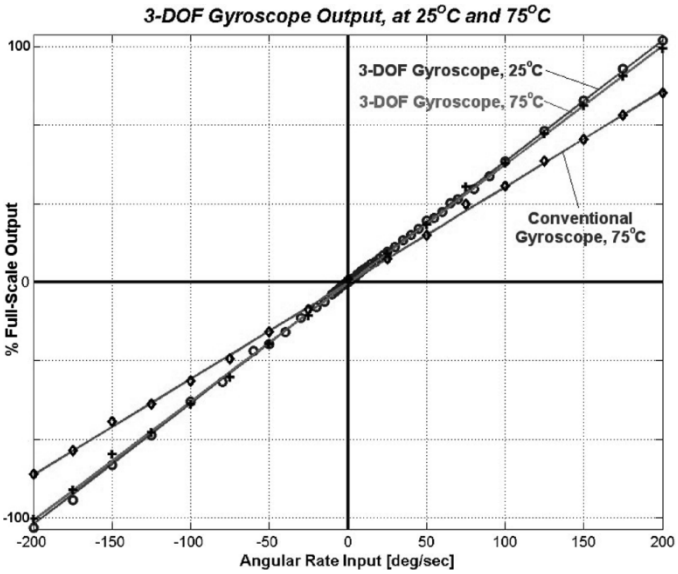

Fig. 13. The measured angular-rate response of the 3-DOF gyroscope and a conventional gyroscope at 25 and 75 °C.

where disturbance-rejection capability is achieved by the mechanical system instead of active control and compensation strategies. The micromachined gyroscopes of this class are expected to yield reliable, robust, low-cost, and high-performance vibratory rate gyroscopes for high-volume applications.

REFERENCES

[1] P. Greiff, B. Boxenhorn, T. King, and L. Niles, "Silicon monolithic micromechanical gyroscope," in *Tech. Dig. 6th Int. Conf. Solid-State Sensors Actuators (Transducers'91)*, San Francisco, CA, Jun. 1991, pp. 966–968.

[2] H. Xie and G. K. Fedder, "Integrated microelectromechanical gyroscopes," *J. Aerosp. Eng.*, vol. 16, no. 2, pp. 65–75, Apr. 2003.

[3] N. Yazdi, F. Ayazi, and K. Najafi, "Micromachined inertial sensors," *Proc. IEEE*, vol. 86, pp. 1640–1658, Aug. 1998.

[4] W. A. Clark and R. T. Howe, "Surface micromachined Z-axis vibratory rate gyroscope," in *Solid-State Sensor Actuator Workshop*, Hilton Head, SC, 1996, pp. 283–287.

[5] A. Shkel, R. Horowitz, A. Seshia, S. Park, and R. T. Howe, "Dynamics and control of micromachined gyroscopes," in *Amer. Control Conf.*, CA, 1999, pp. 2119–2124.

[6] S. Park and R. Horowitz, "Adaptive control for Z-axis MEMS gyroscopes," in *Amer. Control Conf.*, Arlington, VA, Jun. 2001.

[7] R. P. Leland, "Adaptive tuning for vibrational gyroscopes," in *Proc. IEEE Conf. Decision Control*, Orlando, FL, Dec. 2001.

[8] C. Acar, "Robust micromachined vibratory gyroscopes," Ph.D. dissertation, Univ. of California, Irvine, 2004.

[9] C. Acar and A. Shkel, "Non-resonant micromachined gyroscopes with structural mode-decoupling," *IEEE Sensors J.*, vol. 3, no. 4, pp. 497–506, 2003.

[10] C. Acar, C. Painter, A. Schofield, and A. Shkel, "Robust micromachined gyroscopes for automotive applications," in *NSTI Nanotechnology Conf.*, vol. 3, Anaheim, CA, 2005, pp. 375–378.

[11] A. Shkel, R. T. Howe, and R. Horowitz, "Modeling and simulation of micromachined gyroscopes in the presence of imperfections," in *Int. Conf. Modeling Simulation of Microsystems*, Puerto Rico, 1999, pp. 605–608.

[12] J. A. Geen, "A path to low cost gyroscopy," in *Solid-State Sensor Actuator Workshop*, Hilton Head, SC, 1998, pp. 51–54.

[13] W. Geiger, W. U. Butt, A. Gaisser, J. Fretch, M. Braxmaier, T. Link, A. Kohne, P. Nommensen, H. Sandmaier, and W. Lang, "Decoupled microgyros and the design principle DAVED," *IEEE Sensors J.*, pp. 170–173, 2001.

[14] C. W. Dyck, J. Allen, and R. Hueber, "Parallel plate electrostatic dual mass oscillator," in *Proc. SPIE Conf. Micromachining Microfabrication*, vol. 3876, CA, 1999, pp. 198–209.

Cenk Acar was born in Turkey in 1977. He received the B.S. degree in mechanical engineering from Bogazici University, Turkey, and the M.S. and Ph.D. degrees in mechanical and aerospace engineering from the University of California, Irvine.

His current research interests include design, modeling, fabrication, characterization, and control of microelectromechanical systems (MEMS) inertial sensors. He is the first author of more than 20 publications on MEMS inertial sensors. He has ten patents pending. He is currently with BEI Technologies Systran Donner Automotive Division as Senior Inertial MEMS R&D Engineer.

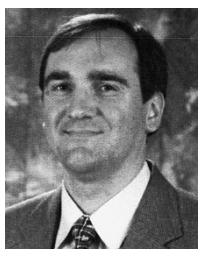

Andrei M. Shkel (S'95–A'98) received the diploma (with excellence) in mechanics and mathematics from Moscow State University, Russia, in 1991 and the Ph.D. degree in mechanical engineering from the University of Wisconsin-Madison in 1997.

He has been on the Faculty of the University of California, Irvine, since 2000, where he is an Associate Professor in the Department of Mechanical and Aerospace Engineering, in the Department of Electrical Engineering and Computer Sciences, and in the Department of Biomedical Engineering. He is also Director of the UCI Micro-Systems Laboratory. After his Ph.D., he joined Berkeley Sensor and Actuator Center (BSAC) as a Postdoctoral Researcher. He then held research and consulting positions in several high-tech and venture companies, including Honeywell Corp., Endevco Inc., MEMSolutions Inc., Solus Microtechnologies, VIP Sensors, Silicon Valley Venture, and Geo-X Corporation. His professional interests, reflected in more than 90 publications, include solid-state sensors and actuators, MEMS-based neuroprosthetics, sensor-based intelligence, and control theory. He has received six U.S. and international patents (13 are pending) on micromachined angle-measuring gyroscope, wide-bandwidth rate gyroscopes, design and fabrication of light manipulators and tunable optical filters, and hybrid surface micromachining processes. He has served on a number of editorial boards, including the *International Journal on Smart Structures and Systems*. He was a Member of the Editorial Advisory Board for *SensorTech* and a member of the Technical Committees of the 2001, 2002, 2003, 2004, 2005, and 2006 SPIE, TMS 2003, and ACC 2001.

Dr. Shkel is an Associate Member of ASME and SPIE. He was Guest Editor for two special issues of the IEEE SENSORS JOURNAL, General Chair of the 2005 IEEE Sensors Conference, and Vice General Chair and Publications Chair of the 2002, 2003, and 2004 IEEE Sensors Conferences. He received the 2005 National Science Foundation CAREER award, the 2002 George E. Brown, Jr., Award and a 2001 Fellowship from the Japanese Advanced Science Institute.